Macromolecules
ARTICLE

Macromolecules **2010**, *43*, 7771–7778 **7771**
DOI: 10.1021/ma101028b

Elongational Rheology and Brillouin Light Scattering of Entangled Telechelic Polybutadiene Based Temporary Networks

Florian J. Stadler,*[,†,⊥] Tim Still,[‡] George Fytas,[‡,§] and Christian Bailly[†]

[†]*Pôle Bio- and Soft Matter (BSMA), Institut de la Matière condensée et des Nanosciences (IMCN), Université catholique de Louvain, Croix du Sud, 1, B-1348 Louvain-la-Neuve, Belgium,* [‡]*Max Planck Institute for Polymer Research, Ackermannweg 10, 55128 Mainz, Germany,* [§]*Department of Materials Science, University of Crete and FORTH, P.O. Box 1527, 71110 Heraklion, Greece, and* [⊥]*Chonbuk National University, School of Semiconductor and Chemical Engineering, 664-14, 1-ga Deokjin-dong, Deokjin-gu, Jeonju, Jeonbuk, 561-756, Republic of Korea*

Received May 8, 2010; Revised Manuscript Received August 9, 2010

ABSTRACT: This article focuses on the characterization of a series of telechelic polybutadienes with acid end groups (PBd−COOH) neutralized with different alkali metal ions by elongational rheometry. Depending on the ion, the material is found to be strain-hardening or not. While the Li^+ ions cause a strain hardening similar to that observed for low density polyethylene, Na^+ and K^+ essentially do not lead to any strain hardening. Rb^+ leads to a different type of strain hardening, like sparsely branched polymers. It is also found that the material behaves brittlely at strain rates $\dot{\varepsilon}$ higher than the crossover frequency ω_c. Additionally, an esterified version of the material and the rubidium hydroxide neutralized PBd−COOH is characterized by Brillouin light scattering to assess the local chain dynamics, being essentially noninfluenced by the ion clusters. The dependence of the longitudinal sound velocity c_l and hence the longitudinal modulus M from the phonon wave vector $\mathbf{q}$ and from the temperature T is compared for two different samples (with and without counterion). It is found that M is insensitive to the presence of the ionic clusters, and therefore, the local chain dynamics are essentially the same for the two model systems and do not play a role in the strain-hardening.

Introduction

Ionomers are a class of polymers with a very high technical potential, composed of a polymeric backbone carrying ionic groups. Electrical charge neutrality is assured by counterions, which can be inorganic, organic, or in some cases polymeric. The most explored systems are acid−base ionomers consisting of hydrophobic chains carrying carboxy group anions neutralized by alkaline metal cations.[1,2] Depending on the degree of neutralization, the ion concentration, and other factors (aging, mechanical history, thermal history, chemical structure, ...), the anions and cations form clusters or multiplets leading to intrachain phase separation.[3]

The random distribution of ionic groups in ionomers along the chain forms a limitation for fundamental studies on the relationship between the dynamics and the phase-separated structure. Interesting models for ionomers consist of so−called "ionic telechelic" polymers. The term "telechelic" refers to chain functionalities exclusively located at the chain end. Often, (and also in the case of the polymers used here) the ionic telechelic ends are carboxyl-groups, but not exclusively. Unlike ionomers, this group of materials has been little studied and remains far less understood. In particular, the viscoelastic behavior in the bulk has rarely been analyzed.[4−9]

In a recent paper, Stadler et al.[10] have studied the linear viscoelastic properties of carboxy-telechelic polybutadiene with a moderate number of entanglements. On the basis of the chemical structure, one might suspect that monovalent ions are not as effective as multivalent ions. Jerome's group[11−16] clearly proved that using divalent ions leads to a structure, which has a terminal relaxation beyond the reach of the experimental methods. In other words, divalent ions more or less cross-link the ionomer (depending in the ionic strength), while monovalent ones reversibly cross-link it; i.e., they slow down the terminal relaxation time significantly. Stadler et al.[10] found a slowing down between factor 343 and 1.6×10^9 in relation to the esterified precursor.

By careful control over the thermo-mechanical history of the samples, they could assess the equilibrium viscoelastic properties and found results on ion dependence which are at odds with previous published literature. They also clearly identified a separate ionic phase glass transition in alkaline metal-neutralized systems, leading to a failure of time−temperature superposition in the plateau modulus region.

Very little is known so far about the nonlinear viscoelastic properties of ionic telechelic polymers. To the best of our knowledge, elongational properties have not been described at all, while some is known for ionomers.[17] In general, the major features in elongational rheology are found at large strains and fast rates. This is where the Trouton ratio (Tr), defined as the ratio of the elongational to the shear viscosity, can deviate from the standard value of three in uniaxial elongation:[18]

$$\eta_e^+(t) = \mathrm{Tr} \times \eta_s^+(t) \tag{1}$$

The so-called *"strain hardening"*, means that $\eta_e^+(t)$ is larger than $3\eta_s^+(t)$, where $\eta_e^+(t)$ is the transient elongational viscosity and $\eta_s^+(t)$ is its counterpart in shear. This leads to high melt stability in processing, which is caused by the stabilization or "self healing" of sample thickness inhomogeneities under flow, and makes the material more tolerant to processing instabilities, thus, widening the processing window.[19]

While a significant number of data exists for elongational rheology of classical covalent polymers, especially polyolefins,[20−26] the elongational behavior of ionomers has received little interest. Conelly et al.[17] found that ionomers can be strain-hardening and

*Corresponding author. E-mail: fjstadler@jbnu.ac.kr. Telephone: +82 63 270 4039. Fax: +82 63 270 2306.

Published on Web 08/31/2010

that an increase of the ion concentration leads to an increase of the amount of strain-hardening. Also a higher ion concentration leads to an earlier occurrence of strain hardening. This dependence of the onset of strain hardening on ion concentration separates ionomers from conventional strain hardening polymers, which, in general, show a "universal" onset of strain hardening around a Hencky strain ε_H of 0.7−1. This leads to the question of the molecular origin of elongational strain hardening in ionic telechelic systems.

Rheological methods alone are neither sufficient to decide about this question, nor the origin of the already observed thermorheological complexity of ionic telechelic systems, in particular whether these effects relate to the local segmental dynamics, as in classical covalent polymers, or are closely linked to the ionic phase. Brillouin light scattering (BLS), the inelastic scattering of light on thermal phonons, is a nondestructive and noninvasive method to determine the longitudinal and transverse sound velocities of a material and by that their mechanical moduli. It will be employed here to explore segmental dynamics and examine whether the observed thermorheological complexity of our telechelic samples arises from heterogeneous local mobility at temperatures well above the glass transition temperature.[27]

The overall objective of this paper is to explore the dynamics of ionic telechelic systems by extending the previous work[10] to elongational rheology and Brillouin light scattering for a set of carboxy telechelic polybutadiene samples with a low number of entanglements, neutralized by various alkaline metal ions. The paper is divided in three main sections: Experimental Section and results for both the BLS and elongational rheology techniques, followed by a conclusion.

Experimental Section

Sample Preparation. The commercially available Hycar CTB 2000 × 162 from Emerald Materials was taken as the base material for the investigations. The terminal COOH groups were neutralized by alkali metal hydroxides in ethanolic solution. Lithium, sodium, potassium, and rubidium hydroxide were used in this study. Next, the solvent was evaporated under ambient conditions until the weight was constant. Additionally, the influence of the COOH-end groups was assessed by esterifying them with ethanol. The precise experimental details are described elsewhere.

Brillouin Light Scattering. In the BLS experiment, two samples have been investigated: The esterified HYCAR 200×162 material ("PBd−COOEt") and the same material neutralized by rubidium hydroxide ("PBd−COOH + RbOH"). Samples of about 1 cm^2 with thickness of 0.5−1 mm have been placed in between two thin glass substrates and fixed in a sample holder that was inserted into the laser beam. Here, an angle-dependent experiment has been performed in order to record the dispersion relation, as well as a temperature-dependent experiment at constant scattering angle.[28] Using a particular transmission scattering geometry for films, where the scattering angle θ is twice the incident reflection angle, the magnitude of the scattering wavevector $q = (4\pi/\lambda) \sin(\theta/2)$ depends on the wavelength λ of the laser beam and θ, but not on the refractive index of the medium.

Elongational Rheology. The rheological testing was performed on a strain-controlled ARES rheometer from TA Instruments. The measurement of the shear viscosity in linear viscoelasticity was already described elsewhere.[29] However, because of the very long time required for the sample to get into equilibrium, the shear viscosity functions used here were taken from the samples in nonequilibrium state (otherwise all elongational samples would have to be equilibrated at elevated T for about 1 week in the rheometer). The shear viscosity function was established using the Cox−Merz rule[30]

$$\eta(\dot{\gamma}) \equiv |\eta^*(\omega)| \quad \text{for } \dot{\gamma} = \omega \tag{2}$$

and the Gleissle mirror rule[31]

$$\eta(\dot{\gamma}) \equiv \eta(1/t, \dot{\gamma} \to 0) \tag{3}$$

using dynamic-mechanical data. $|\eta^*(\omega)|$ is the magnitude of the complex viscosity as a function of angular frequency ω and $\eta(\dot{\gamma})$ is the viscosity function, determined from terminal values of the transient shear viscosity for a given shear rate $\dot{\gamma}$. Thus, $|\eta^*(\omega)|$ can also be taken as the linear reference for the elongational data. The elongational viscosity was measured with the ARES-EVF tool at room temperature and at 50 °C. Contrary to the standard setup, no clamps were used, as the samples were sticky enough that clamping was not necessary. This reduces the risk of experimental artifacts due to the clamps touching each other at large strains ε_H.

Results

Brillouin Light Scattering. The vastly different shear mechanical behavior of the two materials—the PBd−COOH esterified with ethanol (PBd−COOEt) and neutralized with rubidium hydroxide (PBd−COOH+RbOH)[29]—can originate from either strong slowing down of the segmental mobility and/or disruption of the flow because of the clustering of the end groups in PBd−COOH + RbOH. The former possibility can be examined over the relevant temperature range by the measurement of the dynamic longitudinal modulus M^* at GHz frequencies by Brillouin light scattering (BLS).[32] In the rheological experiment, disparity in the local dynamics in PBd−COOH + RbOH and PBd−COOEt would lead to different shift factors $a(T)$.

BLS measures the spectrum of the inelastic scattered light by phonons with wave vector $\mathbf{k}$ equals $\mathbf{q}$, the scattering wave vector, $\boldsymbol{q} = \mathbf{k_s} - \mathbf{k_i}$, which is defined by the difference between the wave vectors of the scattered and incident laser light. For a homogeneous medium over the length scale of the probing wavelength $\sim q^{-1}$, the spectrum consists of a single doublet at $\omega_B = \pm cq$ around the central elastic Rayleigh line with c being the speed of sound with longitudinal (l) or transverse (t) polarization. Since c in soft materials, e.g., polymers, is of the order of 10^3 m s^{-1} and q is in the range $10^6 - 10^7$ m^{-1}, the frequencies $f = \omega_B/2\pi$ fall in the GHz range. BLS measures the dynamic longitudinal modulus

$$M^* = \rho(\omega_B^*/q)^2 \tag{4}$$

where, in general for viscoelastic media

$$\omega_B^* = \omega_B + i\Gamma_B \tag{5}$$

with Γ_B being the line width (half width at half-maximum) of the Brillouin line. Hence, the real and imaginary part of M^* are

$$M' = \rho c_l^2 \tag{6}$$

and

$$M'' = \rho(\Gamma_B/q^2)\omega_B \tag{7}$$

with ρ being the mass density of the material. The longitudinal modulus M can be written as $M = K + (4/3)G$, where K and G are the bulk and shear modulus, respectively; $M^*(\omega) \sim K^*(\omega)$ since G is small compared to the compression modulus K at high frequencies.[33]

Figure 1 shows exemplary spectra of PBd−COOEt at four different temperatures between 35 and 162 °C. The intensity increases with temperature because the compressibility

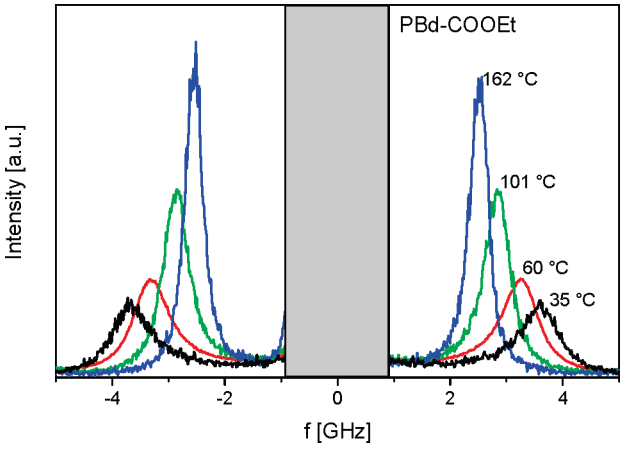

Figure 1. Exemplary BLS spectra of PBd−COOEt at four different temperatures. With increasing temperature, the Lorentzian shaped signals become smaller and are shifted to lower frequencies. All spectra are recorded at $\theta = 70°$ ($q = 0.01355\ \mathrm{nm}^{-1}$).

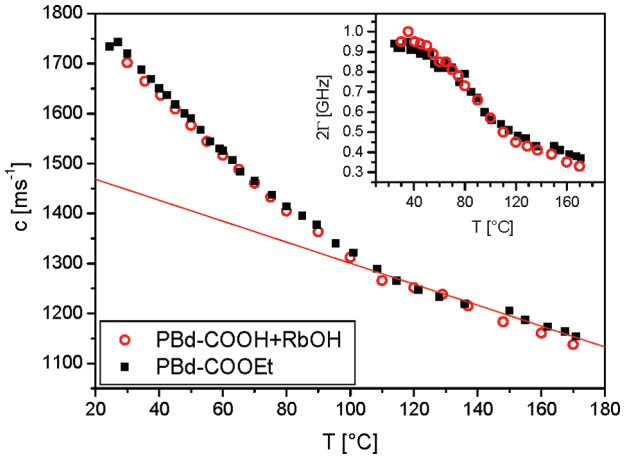

Figure 2. Longitudinal sound velocity of PBd−COOH+RbOH (open circles) and PBd−COOEt (squares) measured by BLS as a function of temperature. Inset: Line width (full width at half-maximum, 2Γ) of PBd−COOH + RbOH (open circles) and PBd−COOEt (squares) measured by BLS as a function of temperature. $\theta = 70°$ ($q = 0.01355\ \mathrm{nm}^{-1}$).

(~$1/K'$) increases with temperature, too, which is evident from the shift of the peak position of the BLS spectra. While the decrease of ω_B is expected due to the reduction of $K' \approx M'$ with temperature, the narrowing of the peak with increasing temperature is counterintuitive. This implies the presence of dispersion in the GHz range, i.e., $\omega_B\tau \approx 1$, where τ is the characteristic segmental relaxation time.[32] The two physical quantities, sound velocity c and sound absorption (~Γ_B) at a single $q = 0.0135\ \mathrm{nm}^{-1}$ ($\theta = 70°$), are plotted as a function of temperature for PBd−COOEt and PBd−COOH+RbOH in Figure 2. The shape of the experimental $c_l(T)$ indicates two distinct variations with temperature. Above about 100 °C, the sound velocity can be represented by a linear fit as a function of T, $c_l(T) = 1510\ \mathrm{ms}^{-1} - 2.1\ \mathrm{ms}^{-1} \times T/°\mathrm{C}$, suggesting a liquid behavior, i.e., $\omega_B\tau \ll 1$ ($\omega_B = c_l q$) for both materials. Below $T \approx 100$ °C, $c_l(T)$ increases faster with decreasing temperature than predicted by the linear dependence above about 100 °C due to the dispersion in $K^*(\omega)$. This dispersion consistently leads to a stronger increase of Γ_B with decreasing temperature below about 100 °C for both materials as seen in the inset of Figure 2. Since $\tau(T)$ increases with decreasing temperature, the reduced quantity $\omega_B\tau \approx 1$ at a temperature T_m, at which the line width Γ_B exhibits its maximum value.

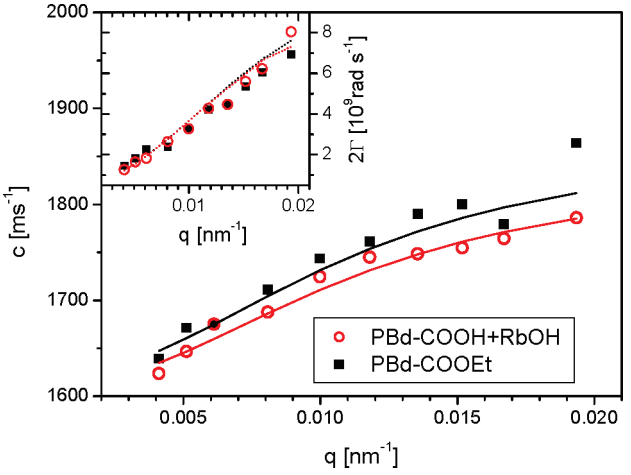

Figure 3. Longitudinal sound velocity and dissipation expressed in the line width 2Γ (inset) of PBd−COOH + RbOH (open circles) and PBd−COOEt (squares) measured by BLS as a function of the phonon wave vector q at room temperature. The solid lines denote their representation by eqs 9 and 10.

On the basis of the same − within the experimental error − dependence of the experimental $c_l(T)$ and $\Gamma_B(T)$ of Figure 2, both systems display the same local dynamics with $\tau \approx 40$ ps at ambient temperature.

The softening of the temperature dependent longitudinal modulus $M(T)$ at high frequencies occurs at two temperatures: Near and above the glass transition temperature ($T_g \approx -79$ °C), $M(T)$ decreases due to the density and compressibility changes crossing T_g, at which $\omega_B\tau \gg 1$ (solid-like behavior), and at the crossover temperature $T_m > T_g$, at which $\omega_B\tau \approx 1$, due to the viscoelastic behavior. The system exhibits liquid-like behavior when the local segmental dynamics become faster than ω^{-1}, i.e., $\omega\tau < 1$ at $T > T_m$. A rough estimate of T_m can be obtained from the WLF equation

$$\tau = \tau_0 \exp\left[\frac{\Delta E}{\mathrm{R}(T - T_0)}\right] \tag{8}$$

where $T_0 = T_g - c_2 \approx T_g - 50$ K, ΔE is the energy barrier, R the gas constant, and $\tau_0 \approx 10^{-13}$ s is the temperature at which $\tau = 1/\omega_B$, with $\omega_B = 2\pi f$ and $f \approx 5$ GHz. The experimental value of T_m is captured with the reasonable value of $\Delta E \approx 7.5\ \mathrm{kJ\ mol}^{-1}$.

The phonon dispersion as a function of temperature at a constant q should also be manifested isothermally as a function of q. This is a rather rare experiment since an angular dependent BLS is required.[27] Figure 3 shows the small but discernible dispersion of the sound velocity at hypersonic frequencies far above T_g. Assuming a single segmental relaxation time τ, the normalized dispersion of M' is given by

$$r - 1 = (R - 1)\frac{(\omega_B\tau)^2}{1 + (\omega_B\tau)^2} \tag{9}$$

where $r \equiv (M'/M'_0)^2$ and $R \equiv (M'/M'_\infty)^2$ with M'_0 and M'_∞ are the limiting values of M' at low ($\omega_B\tau \ll 1$) and high frequencies ($\omega_B\tau \gg 1$), respectively. Solving eq 9 for the sound velocity c as a function of q, we obtain:

$$c^2 = \frac{\{(c_0^2 q^2\tau^2 - 1) + [(1 - c_\infty^2 q^2\tau^2)^2 + 4c_0^2 q^2\tau^2]^{1/2}\}}{(2q^2\tau^2)} \tag{10}$$

where c_0 and c_∞ are the limiting values of c at low and high frequencies. The solid line in Figure 3 denotes the representation

of the experimental c using $c_0 = 1600-1620$ m s^{-1}, $c_\infty = 1800-1870$ m s^{-1} and $\tau = 30-50$ ps. The sound velocity dispersion is relatively weak, i.e., $R = 1.25-1.33$, but is also discernible in the hypersonic sound dissipation $\Gamma_B = (M''/M')\omega_B$ expressed by

$$\Gamma_B = \Gamma_0 + \frac{(R-1)c_0^2 q^2 \tau}{1+(cq\tau)^2} \quad (11)$$

where Γ_0 accounts for additional source of dissipation. The line width Γ_B obtained from the deconvolution of the experimental BLS spectra with the instrumental function is shown in the inset to Figure 3 as a function of the phonon wave vector. The dotted line denotes the representation of the experimental line widths by eq 11 using the relaxation parameters (c_0, c_∞, and τ) in the same range used for the description of the sound velocity data.

A rationalization of this finding, which is relevant for the rheological behavior of these systems, is the relatively large average distance (~9 nm) between the crossing points between the telechelic clusters in PBd−COOH + RbOH, exceeding the local cooperative length (~1 nm) associated with the segmental dynamics[34] and the fraction of "slow" segments next to the clusters is small. Finally, the sound velocity data in Figure 2 indicate that the compression modulus $K \approx \rho c_l^2$ in the two systems over the range 25−170 °C is the same assuming similar densities. On the contrary, the shear modulus of the two systems measured at much lower frequencies by shear rheology is very different.[29] It was shown that the terminal regime of the different telechelic ionomers samples is identical when applying a shift factor, depending on the ion.[29] This confirms that the terminal behavior, i.e., the state of complete mobility of the chains is identical. The clusters only slow it down by forming a temporary network. The BLS results confirm this finding.

Elongational Rheology. The elongational rheology of telechelic systems is a new field, which has not been explored in detail before. Because of the long equilibrium time of the samples discussed here, it is not possible to anneal the elongational samples to fully reach equilibrium conditions. For this reason, the samples were annealed in bulk and then cut into shape, which slightly damages the annealed structure. Additional annealing in the rheometer was not performed (otherwise sagging would destroy the defined geometry), which leads to slightly different rheological properties in the linear regime in comparison to the samples in equilibrium.[29] Although, it would be desirable to use the equilibrium structured samples, this was not done. Annealing the cut samples for several days will lead to some sample deformation; this is even more true for loading the sample into the rheometer and annealing it in situ. Even doing that for the Rb^+-neutralized sample, after several hours at room temperatures a noticeable sagging is obvious even at room temperature (this was the limiting factors for the elongational rate at 50 °C). Hence, annealing the sample in situ is not possible.

Thus, the linear viscoelastic data used as the linear reference of these samples was determined from shear samples under the same conditions. The linear viscoelastic envelope was not measured by a start-up flow but by frequency sweeps applying the Cox−Merz rule[30] and the Gleissle mirror rule.[31] The possibility to do that was proven elsewhere for linear and long-chain branched polymers.[21]

The data relative to the Rb^+-neutralized sample were measured at room temperature (23 °C) and 50 °C as the crossover frequency of this sample is at very low frequencies, and thus the transition from brittle to ductile behavior cannot be very well observed otherwise. The three lowest strain rates in Figure 4d, therefore, are measured at 50 °C and shifted to 23 °C using a shift factor a_T of 0.14, which is much lower than the shift factor observed in equilibrium state for this sample ($a_T = 0.025$) and again shows the large time dependence of the shift factors.[29] The strain rates of the samples measured at 50 °C are given in ***bold italics***. This comparison is also possible, because the same shift factors can used in elongation and in shear, which was proven to be possible before for LDPE and PS.[22,23]

Because of the high viscosity of the alkali metal ion-neutralized samples, the zero shear-rate viscosity η_0 of the samples is in the order of about one million Pa s to several billion Pa s, depending on the ion, sagging does not pose any problem to the experiments, as long as the strain rate is not below a certain threshold, which is sample specific, i.e., η_0 specific. However, because of the low viscosity the virgin material as well as the esterified (PBd−COOEt) and the butyl amine samples could not be tested in elongation.

Before going to the elongational rheology, a few words concerning the molecular structure and architecture are necessary for a good understanding of the data. On the basis of earlier observations from SAXS and FT-IR reported before, we know that the neutralized samples have a biphasic structure. The matrix phase consists of the PBd-main chains, and the end groups form clusters together with the counterions (see scheme in Stadler et al.). These clusters are separated by about 9 nm—depending on the counterion. This is significantly less than the stretched length of a chain, which would be around 20 nm.

If we consider two clusters in the direction of an elongational deformation, then full extension of the chains connecting them induces a maximum cluster separation distance of 20 nm. In equilibrium, this intercluster distance is approximately 8 nm, so a Hencky strain of ≈0.9 is required. Besides the elongational viscosity itself, also the elongation at the onset of instability, defined by the decrease of the apparent viscosity as a function of time to values significantly below the shear envelope, plays an important role in understanding the elongational rheology.

Figure 4 shows the elongational viscosities as a function of time for different strain rates. The first obvious difference is that PBd−COOLi and PBd−COORb lead to strain hardening (Figure 4a,d), while PBd−COONa and PBd−COOK do not show signs of strain hardening in a wide range of strain rates (Figure 4b,c).

This ion dependence of the strain hardening might seem a little bit awkward at a first glance, as this does not follow a logical order, but the results are very clear, so that an experimental artifact can be excluded. When looking closer at the highest strain rates, it becomes obvious that all materials show a tendency to strain hardening, which, however, is only ill-developed due to the low elongation at break ε_H^{max} (typically 0.7−1) of these samples at high strain rates $\dot{\varepsilon}$. This issue is discussed later in the paper.

A comparison of the strain hardening of PBd−COOLi and PBd−COORb shows that the pattern of strain-hardening is different, which is a first hint that the physical mechanism of the strain hardening is different for these samples. The Li^+-neutralized sample (PBd−COOLi) shows an increase of strain hardening with rising strain rate $\dot{\varepsilon}$, when disregarding the data at the highest strain rates, where the elongation at break is too low to fully develop the strain hardening. This behavior is quite similar to that of low density polyethylene (LDPE), although the level of strain hardening is a little lower. In LDPE, this behavior is associated

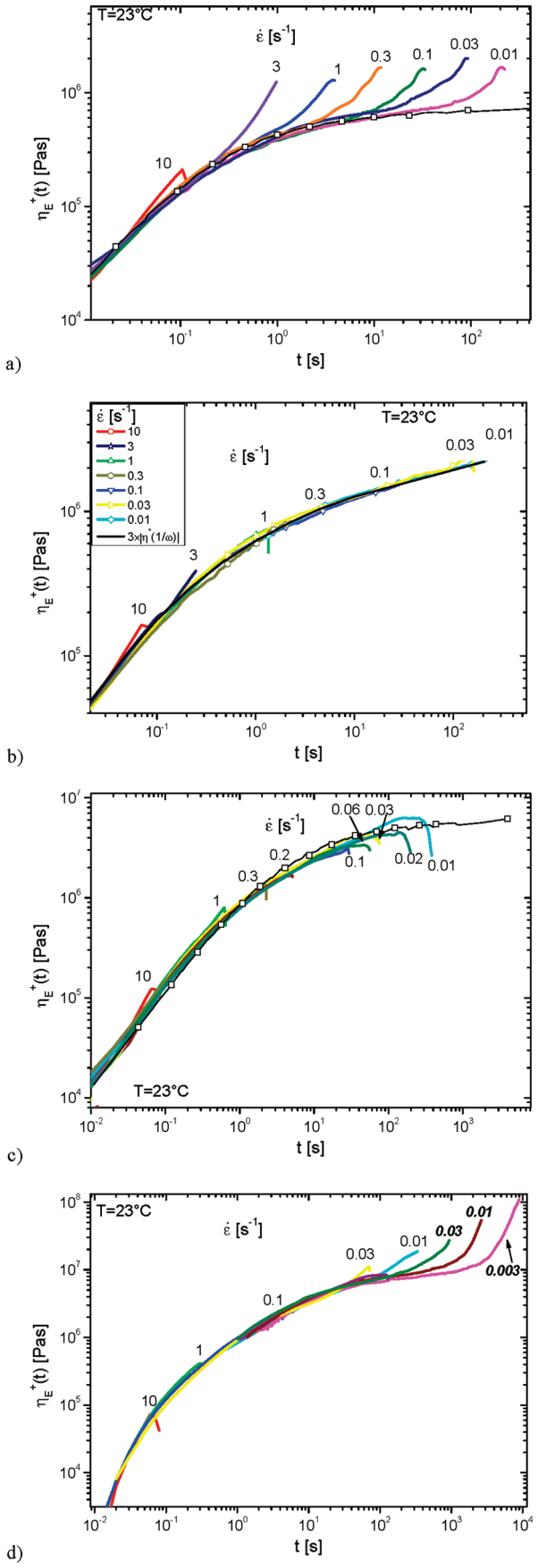

Figure 4. Elongational rheological data of (a) PBd−COOLi, (b) PBd−COONa, (c) PBd−COOK, and (d) PBd−COORb. The large figures give the elongational viscosity η_E^+ as a function of time for different Hencky strain-rates.

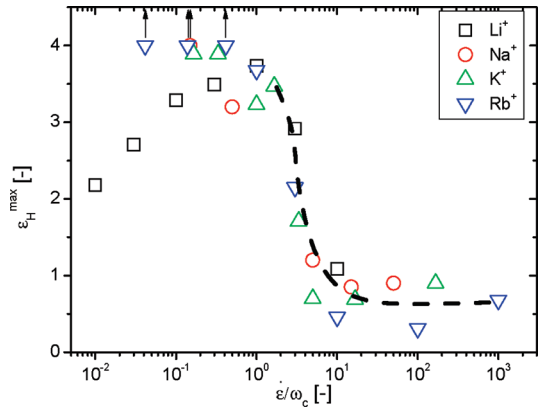

Figure 5. Maximum obtained Hencky strain ε_H^{max} as a function of strain rate normalized by crossover frequency $\dot{\varepsilon}/\omega_c$. Line added to guide the eye.

with highly hierarchical branched chains with relatively short segmental relaxation times.[35,36] The Rb^+-neutralized sample, in contrast shows an increase of the strain hardening with decreasing strain rate $\dot{\varepsilon}$, a behavior usually found for lightly branched systems with high segmental relaxation times, such as metallocene long chain branched PE.[35,36] Also the degree of strain hardening of this sample is lower than that of the Li^+-neutralized sample, which is also typical for this type of strain hardening.

It was mentioned before that the strain at break depends to a large degree on the strain rate. To illustrate this in detail, Figure 6 shows the obtained Hencky strains at break ε_H^{max} as a function of the strain rate normalized by the crossover frequency $\dot{\varepsilon}/\omega_c$. This normalization accounts for the sample dependent characteristic terminal relaxation time. Unlike in classical covalent polymer melts, here two "rubbery" plateaus are observed of which the upper one corresponds to the telechelic network fixed by the *glassy aggregates* and the lower one is equivalent to the normal rubbery plateau in polymer melts. The "upper rubbery plateau" is caused by the fact that the ion clusters are glassy, i.e., they can be considered as *glassy aggregates* firmly cross-linking the rubbery matrix. The "lower" rubbery plateau corresponds to the rubbery plateau for conventional polymers. In this regime, the ion clusters are soft enough that they can be considered to be nonpermanent cross-linkers. The crossover frequency marks the end of the lower rubbery plateau.[1,2,29]

Figure 5 shows that around $\dot{\varepsilon}/\omega_c > 3$ a Hencky strain at break ε_H^{max} around 0.7 is found followed by a very sharp increase around $\dot{\varepsilon}/\omega_c = 3$ to $\varepsilon_H^{max} > 4$. $\varepsilon_H = 4$ is the maximum deformation which can be reached accurately with the setup used. These properties are ion independent for $\dot{\varepsilon}/\omega_c > \approx 0.8$. At smaller normalized strain rates, no break is observed for PBd−COONa, PBd−COOK, and PBd−COORb (indicated by the arrows in Figure 5). For most samples, a break is not found when stretching the sample to $\varepsilon_H \approx 8$, which can be done by winding the sample up twice with the EVF. Because this automatically changes the drum diameter and the corresponding kinematic equations, it is not possible to quantify the viscosity, but it is possible to state that many samples even survive a stretch to $\varepsilon_H \approx 8$, which is truly exceptional, as most polymeric samples become unstable around $\varepsilon_H = 2-4$!

The PBd−COOLi-neutralized sample differs from the other samples in this respect. It shows a decreasing strain at break with decreasing $\dot{\varepsilon}/\omega_c$. This deviation might seem counterintuitive, but indicates clearly that the Li^+-ion has a different interaction with the carboxy-group than the other ions.

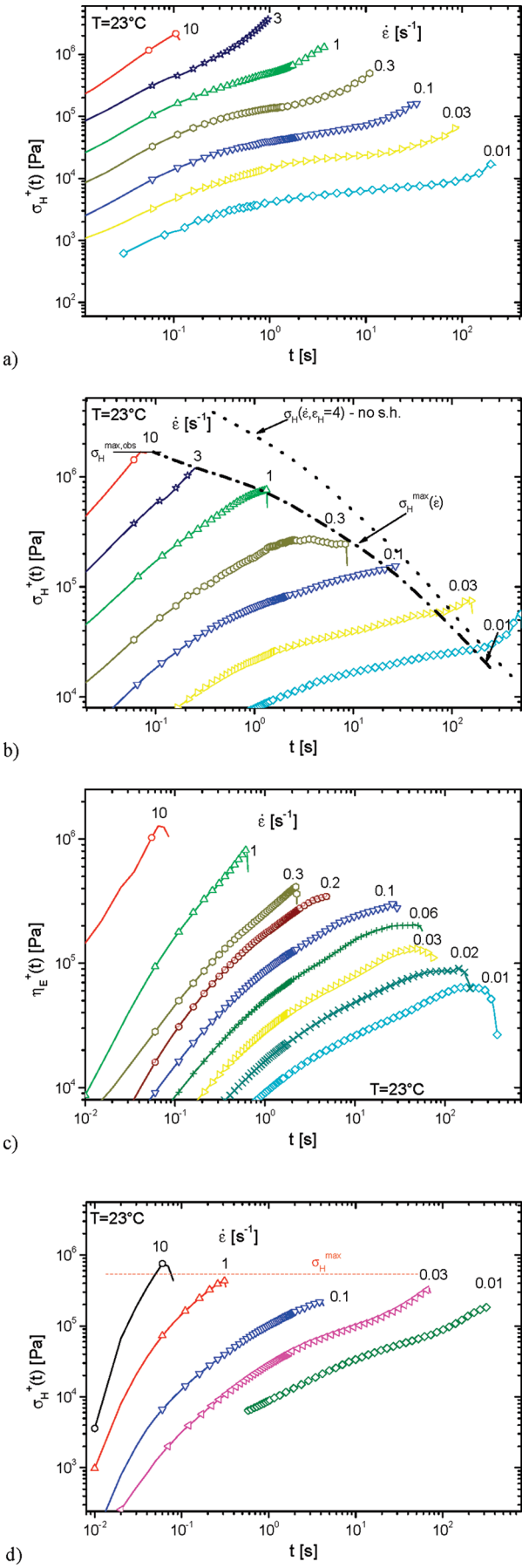

Figure 6. Elongational stress as a function of time of (a) PBd−COOLi, (b) PBd−COONa, (c) PBd−COOK, and (d) PBd−COORb.

In fact, it has been regularly reported that Li^+-neutralized ionomers seem not to adhere to the classical relationships found in other ionomers, which is due to the partially covalent character of the Li^+-ion.[37]

The long-period of the materials, i.e. the average cluster separation distance, is around 9 nm with clusters around 1 nm in size.[29] The stretched chain length of the PBd-main chains is ≈25 nm with respect to M_n and ≈50 nm with respect to M_w. If we assume that a chain connects two clusters in the direction of the strain, the Hencky strain for elongating the coiled chain to its stretched length is between $\varepsilon_H = 1.1$ with respect to M_n and $\varepsilon_H = 1.8$ with respect to M_w.

This explains the low elongation of break for $\dot{\varepsilon}/\omega_c > 3$. In this regime, the clusters behave glassy, i.e., as rigid cross-linkers of the chains attached to them. This has two consequences. First, the strong binding of the cross-linkers enable a high strain hardening. Second, only the onset of strain hardening is observed because the stretched chains are so stiff that the brittle glassy ion-clusters quickly disintegrate under strong elongational stress. So the onset of breaking occurs as soon as soon as the first PBd-chains are stretched between two clusters, since the stress is then exerted on the clusters, which, of course, break quickly under such circumstances.

If we assume that the bond between the Li^+-ion and the telechelic carboxy-groups is covalent, the elongation at break should be in the range around $\varepsilon_H = 1.8$, because the weight-average of the chains is fully elongated then. However, the data is collected in the terminal regime. So this physical process cannot be the conclusion. Nevertheless, the fact that the instability only occurs for the Li^+-neutralized sample and that the type of strain hardening also differs, must mean that the interaction in the ion-clusters of the Li^+-neutralized sample is fundamentally different from the other ions. The somewhat covalent nature of Li^+-ions could be the reason for the instability. Possibly because the deformation of the ion-clusters is not as smoothly as for the other ions and, thus, the ion-clusters destabilize under elongation.

The maximum Hencky strain ε_H observation can also be interpreted in the following way. At high elongational rates, the sample rips apart approximately at the time when the Hencky stress σ_H reaches the value of the plateau modulus. This can be interpreted as the rupture strength of the telechelic network. This rupture strength σ_H^{max} is found to be in the order of approximately 10^6 Pa (Figure 6). Because of the nonlinear shape of the elongational viscosity η_e^+, it is not possible to predict the value of σ_H at a high Hencky strain ε_H (e.g., 4), but it will be higher than expected from linear viscoelasticity, as the materials have a tendency to strain-harden at high strain rates.

It is important to note that in this plot the data at different strain rates do not collapse onto each other as is observed for the elongation viscosity (in the absence of strain hardening).

The plot for the PBd−COONa (Figure 6b) additionally shows the maximum stress expected from the shear data, denoted as the dashed line ($\sigma(\varepsilon_H = 4)$), acquired under the assumption that no strain hardening occurs. The dashed dot line in Figure 6b represents the actually measured maximum stress as a function of strain rate $\sigma_H^{max}(\dot{\varepsilon})$. In an ordinary covalent polymer, the actual measured maximum stress is never below the stress predicted from shear data. In case of the samples tested here, the two lines approach each other with increasing time/decreasing strain rate $\dot{\varepsilon}$ and even cross each other at the longest times, but the measured stress is essentially always below the stress predicted from shear data. This means that the samples cannot withstand the same stress a normal polymer can. At lower strain rates $\dot{\varepsilon}$, however,

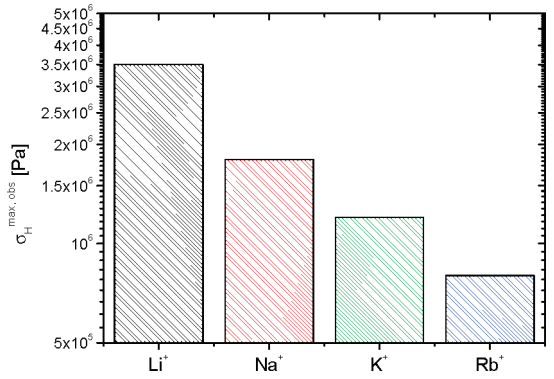

Figure 7. Maximum observed stress for the different PBd-COO^- samples.

this lack of stability of the polymer is not as relevant because the stresses are much lower and, hence, the cohesion of the network is not problematic.

This is different from conventional materials, which can be stretched to values of σ_H^{max} much higher than the plateau modulus. E.g. high molecular PIB could be stretched with up to 1.6×10^8 Pa, which is 500 times G_N^0.[38] This difference highlights the weak nature of the bonds in temporary network in comparison to entanglements (and even more to covalent networks).

Interestingly, the maximum stress observed $\sigma_H^{max,obs}$ decreases with increasing atomic number of the ion used. The strength of the bond can be qualitatively related to the energy of first ionization. $\sigma_H^{max,obs}$, the stress at break at high strain rates, is higher for higher ionization energies, i.e., the stronger the cohesive forces of the chains and the ions in the clusters.

This finding makes sense, as a high cohesive strength of the clusters corresponds to a high macroscopic strength of the material. This statement is only possible, however, because the concentration of supramolecular links is not varied in this sample series. The relatively large difference between Li^+ and Na^+ is possibly a consequence of the much more covalent nature of Li^+.[37]

This "full stretch" Hencky strain ε_H is found to play a significant role in two respects. First, it is the average elongation at break ε_H^{max} observed for samples stretched faster than their terminal relaxation rate. Second, it is the onset of strain hardening.

As the clusters can be considered to be static cross-linkers for such high stretching rates, the elongational test corresponds to the pullout of chains out of the clusters. In other words, the stretch rates probe the cohesive strength of the clusters. As can be seen from Figure 7, this cohesive strength is ion dependent. Because the geometry of the clusters being pulled apart is ill-defined, a more quantitative analysis is not possible but the qualitative comparison between the different ions shows a clear trend.

Conclusions

Although the onset of strain hardening is similar as observed for conventional long-chain branched polymers ($\varepsilon_H \approx 0.7-1$), the origin of this behavior is quite different. At $\varepsilon_H \approx 0.9$, the ionic telechelic chains will be—at least some of them—fully stretched. If the strain rate $\dot{\varepsilon}$ is below the crossover frequency ω_c, i.e., the test is performed in the terminal regime, the clusters can no longer be considered to be permanent cross-linkers, but dynamic ones. Hence, the chain ends can dynamically migrate in and out of the clusters (e.g., by Brownian motion), which in turn is observed macroscopically as a transition from rubbery to liquid state. This mobility of the clusters leads to an increase of the maximum stretch, because the most stretched chains can relax their tension by moving out of the cluster. However, the release of COO^--chain ends from an ionic cluster into the hydrophobic main phase is a thermodynamically unfavorable process. The balance between Brownian motions and the external mechanical force governs whether the sample is strain hardening or not. If the external force is very high in comparison with Brownian motions, the sample is strain hardening, if the Brownian motions exert about the same force on the chain ends as the external force, the material is not strain-hardening. In other words, the sample is strain hardening as long as the clusters are stable enough to resist flow to a degree that it also resists stretching them. This balance is summarized in Table 1.

Table 1. Qualitative Assessment of the Occurrence of Strain Hardening

cohesive strength of the cluster	mechanical behavior
weak	fluid-like, non-strain-hardening
medium	viscoelastic to weakly rubbery, strain hardening
high	rubbery, brittle at $\varepsilon_H >$ chain stretch, potentially strain-hardening, but too brittle to probe

The given description is in agreement with the results of the performed BLS measurements. While the strain hardening behavior is clearly dependent on the clusters, the segmental dynamics are unchanged. This result underlines that only the dynamics in the relatively small (compared to the whole sample volume) clusters influence the rheological behavior, while nearly all segments in the PBD chains that are not in direct contact with a cluster show the same segmental motion.

For PBd−COOLi, the cohesive strength of the cluster is quite high ($\sigma_H^{max} \approx 3.5$ MPa), and the cluster mobility is also high. This leads to strain hardening especially at $\dot{\varepsilon}$ slightly below ω_c. PBd−COORb has a much lower cohesive strength but much better ordered clusters. This leads to significantly longer relaxation times (by about a factor of 300 in equilibrium in comparison to Li^+), as a high number of different chains have to move to allow a high stretch. It also leads to destructuring of the ion clusters at high stretch levels. As this destruction of ordered structures absorbs a lot of energy, the material is strain hardening as well. But the strain hardening only occurs at low strain rate $\dot{\varepsilon}$. The reason is that the characteristic relaxation time of the "cluster dissolution process" is much longer than the one of PBd−COOLi.

This collective mobility for PBd−COORb requires significantly more time than the "ripping out" of individual chains we believe to occur in PBd−COOLi. The consequence is that the strain hardening grows with decreasing strain rate/increasing relaxation time, allowing for some reordering and healing of microcracks. For the Na^+- and K^+-neutralized samples, the balance between mobility and cohesion leads to a flow behavior without strain hardening. In other words, the cluster do not stick together sufficiently to pose the additional resistance necessary to create strain hardening.

Summary

In summary, the materials tested in this paper are not networks in the strict sense, as they possess a terminal regime. Therefore, the ion clusters have to be considered as dynamic structures, which can be broken apart by strong deformation and that reform slowly. Hence, it is likely that not all polar groups reside in the ionic clusters − even in equilibrium state.

It is found for all samples that the stretchability of the sample depends highly on the inverse terminal relaxation time (= the crossover frequency ω_c). At shorter inverse relaxation times than

the applied strain rate $\dot{\varepsilon}$ (in the rubberlike regime), the material is quite "brittle",[39] while in the terminal regime a very high extensibility is found. The finding of the "brittleness" in the rubbery regime is different from conventional polymers, which generally show a pretty high stability in the rubbery plateau. The interpretation is that in the terminal regime, the individual chain ends ($-COO^-$ groups) can move in and out of the clusters. This degree of freedom makes the material flowable (as opposed to a normal rubber) and enables high deformations without mechanical failure. At higher rates, corresponding to the dynamics in the rubbery plateau, this mobility is not possible, and therefore, an unstable elongational flow is observed, as the chain ends pulled out from a cluster do not have enough time to return to another cluster.

Acknowledgment. F.J.S. acknowledges financial support from the "Actions de Recherches Concertées" of the "Communauté Française de Belgique".

References and Notes

(1) Tant, M. R.; Mauritz, K. A.; Wilkes, G. L., *Ionomers - synthesis, structure, properties and applications*; Blackie Academics & Professional: London, 1997.
(2) Eisenberg, A.; Kim, J. S., *Introduction to Ionomers*; Wiley: New York, 1998.
(3) Eisenberg, A.; Hird, B.; Moore, R. B. *Macromolecules* **1990**, *23*, 4098–4107.
(4) Broze, G.; Jerome, R.; Teyssie, P. *Macromolecules* **1981**, *14*, 224–225.
(5) Broze, G.; Jerome, R.; Teyssie, P.; Marco, C. *Macromolecules* **1983**, *16*, 1771–1775.
(6) Broze, G.; Jerome, R.; Teyssie, P.; Marco, C. *Macromolecules* **1983**, *16*, 996–1000.
(7) Broze, G.; Jerome, R.; Teyssie, P.; Marco, C. *Macromolecules* **1985**, *18*, 1376–1382.
(8) Davidson, N. S.; Fetters, L. J.; Funk, W. G.; Graessley, W. W.; Hadjichristidis, N. *Macromolecules* **1988**, *21*, 112–121.
(9) Fetters, L. J.; Graessley, W. W.; Hadjichristidis, N.; Kiss, A. D.; Pearson, D. S.; Younghouse, L. B. *Macromolecules* **1988**, *21*, 1644–1653.
(10) Stadler, F. J.; Schumers, J.-M.; Fustin, C.-A.; Gohy, J.-F.; Pyckhout-Hintzen, W.; Bailly, C. *Macromolecules* **2009**, *42*, 6181−6192.
(11) Broze, G.; Jerome, R.; Teyssie, P. *Macromolecules* **1982**, *15*, 1300–1305.
(12) Broze, G.; Jerome, R.; Teyssie, P. *Macromolecules* **1982**, *15*, 920–927.
(13) Broze, G.; Jerome, R.; Teyssie, P. *Macromolecules* **1981**, *14*, 224–225.
(14) Broze, G.; Jerome, R.; Teyssie, P.; Marco, C. *Macromolecules* **1985**, *18*, 1376–1382.
(15) Broze, G.; Jerome, R.; Teyssie, P.; Marco, C. *Macromolecules* **1983**, *16*, 1771–1775.
(16) Broze, G.; Jerome, R.; Teyssie, P.; Marco, C. *Macromolecules* **1983**, *16*, 996–1000.
(17) Connelly, R. W.; Mcconkey, R. C.; Noonan, J. M.; Pearson, G. H. *J. Polym. Sci. Polym. Phys.* **1982**, *20*, 259–268.
(18) Meissner, J.; Stephenson, S. E.; Demarmels, A.; Portmann, P. *J. Non-Newtonian Fluid Mech.* **1982**, *11* (3−4), 221–237.
(19) Münstedt, H.; Steffl, T.; Malmberg, A. *Rheol. Acta* **2005**, *45*, 14–22.
(20) Meissner, J. *Rheol. Acta* **1969**, *8*, 78–88.
(21) Stadler, F. J.; Nishioka, A.; Stange, J.; Koyama, K.; Münstedt, H. *Rheol. Acta* **2007**, *46*, 1003−1012.
(22) Stadler, F. J.; Becker, F.; Kaschta, J.; Buback, M.; Münstedt, H. *Rheol. Acta* **2009**, *48*, 479−490.
(23) Münstedt, H.; Laun, H. M. *Rheol. Acta* **1979**, *18*, 492–504.
(24) Münstedt, H.; Gabriel, C.; Auhl, D. *Abstr. Pap. Am. Chem. Soc.* **2003**, *226*, U382–U382.
(25) Bach, A.; Almdal, K.; Rasmussen, H. K.; Hassager, O. *Macromolecules* **2003**, *36*, 5174–5179.
(26) Nielsen, J. K.; Rasmussen, H. K.; Almdal, K.; Hassager, O. In *Elongational viscosity of multiarm pom-pom polystyrene*. Presended at the 78th meeting of the Society of Rheology, Portland, ME, 2006.
(27) Voudouris, P.; Gomopoulos, N.; Le Grand, A.; Hadjichristidis, N.; Floudas, G.; Ediger, M. D.; Fytas, G. *J. Chem. Phys.* **2010**, *132*, 074906.
(28) Cheng, W.; Sainidou, R.; Burgardt, P.; Stefanou, N.; Kiyanova, A.; Efremov, M.; Fytas, G.; Nealey, P. F. *Macromolecules* **2007**, *40*, 7283–7290.
(29) Stadler, F. J.; Schumers, J.-M.; Fustin, C.-A.; Gohy, J.-F.; Pyckhout-Hintzen, W.; Bailly, C. *Soft Matter* **2008**.
(30) Cox, W. P.; Merz, E. H. *J. Polym. Sci.* **1958**, *28*, 619–622.
(31) Gleissle, W. Short-term measurements for determining the flow properties of plastics up to the highest shearing rates. In *Praktische Rheologie an Kunststoffen*; Karlsruhe, Germany, 1978.
(32) Floudas, G.; Alig, I.; Fytas, G. *Polymer* **1991**, *32*, 2307.
(33) Kanetakis, J.; Fytas, G.; Hadjichristidis, N. *Macromolecules* **1991**, *24*, 1806–1812.
(34) Doxastakis, M.; Theodorou, D. N.; Fytas, G.; Kremer, F.; Faller, R.; Muller-Plathe, F.; Hadjichristidis, N. *J. Chem. Phys.* **2003**, *119*, 6883–6894.
(35) Auhl, D.; Stange, J.; Münstedt, H.; Krause, B.; Voigt, D.; Lederer, A.; Lappan, U.; Lunkwitz, K. *Macromolecules* **2004**, *37*, 9465–9472.
(36) Gabriel, C.; Münstedt, H. *J. Rheol.* **2003**, *47*, 619–630.
(37) Weiss, R. A.; Zhao, H. *J. Rheol.* **2009**, *53*, 191–213.
(38) Stadler, F. J.; Burhin, H.; Dhole, S.; Bailly, C. *Rheol. Acta* **2008**.
(39) "Brittle" is a relative term considering a Hencky strain at break ε_H^{max} of 1, i.e., a Cauchy strain (engineering strain) of 170%.